DOI:
10.1039/C7NR03533K

Document Version
Peer reviewed version

Structural stability and uniformity of magnetic Pt_{13} nanoparticles in NaY zeolite

Cono Di Paola[1], Luca Pavan[1], Roberto D'Agosta[*2,3], and Francesca Baletto[†1]

[1]Department of Physics, King's College London, London, WC2R 2LS, United Kingdom
[2]Nano-bio Spectroscopy Group and ETSF Universidad del Pais Vasco, CFM CSIC-UPV/EHU, E-20018 Donostia-San Sebastian, Spain
[3]IKERBASQUE, Basque Foundation for Science, E-48013 Bilbao, Spain

September 8, 2017

Abstract

Based on first-principles calculations, the structural stability and magnetic variety of Pt_{13} nanoparticles encapsulated in a NaY zeolite are investigated. Among 50 stable isomers in the gas phase, due to geometrical constraints, only about 1/3 of those clusters can be inserted in the zeolite pores. Severe structural rearrangements occur depending on whether the solid angle at the Pt vertex bound to the super-cage is larger than 2 sr (i.e., icosahedron). The most relevant example is the structural instability of the icosahedron and, when including van der Walls dispersion forces the opening of the gas phase global minimum towards a new L-shaped cubic wire, otherwise unstable. The total magnetisation of the encapsulated Pt_{13} decreases due to the stabilisation of less coordinated isomers, with the majority of clusters characterised by a total magnetisation of 2 μ_B, while the majority of free clusters exhibits a threefold value. This analysis allows to understand the magnetic behaviour observed in recent experiments through the variety of the isomers which can be accommodated in the zeolite pore.

Introduction

Within the last few decades, the number of studies related to metallic nano-particles (NPs) has dramatically increased because of potential applications in catalysis, magnetic and optical devices, and nanomedicine.[1,2] One of the main challenges in this field of nanoscience is addressing the structure-property relationship of a structurally uniform sample of metallic NPs in a well defined size range.[3,4] For example, a large magnetic moment in NPs can be determined by the local atomic arrangement surrounding vertex atoms.[5] Here, we investigate how the magnetic properties can depend on the geometrical variety of the sample induced also by the external environment where the NPs are embedded. We will take as a paradigmatic example the case of encapsulated Pt nano-structures in NaY zeolite. These systems are playing a central role in the fabrication of electrochemical devices,[6] including lithium batteries,[7] because Pt-NPs drastically accelerate various chemical reactions of industrial interest.[8,9] Furthermore, Pt-nanosystems, as clusters, nanowires, and thin films, exhibit a magnetic behaviour,[10–13] as a consequence of their broken translation symmetry and, generally a reduced coordination number (CN) has been observed.[14] Recent SQUID measurements of Pt-NPs consisting of 13±2 atoms and encaged in faujasite-Na zeolites report a stable high spin state between $S = 2$ and $S = 3$, equivalent to a total magnetic moment of 4-6 μ_B,[15,16] whereas XMCD studies have indicated a total magnetization peak of 5.9 μ_B.[17,18] In any event, the experimental data sample is not uniformly magnetic; only a small fraction of the nominal Pt-load, specifically 15-20% as measured by XMCD spectroscopy and 30% as measured by SQUID magnetometry is magnetic. Furthermore, 3D electron tomography has provided insights into

*roberto.dagosta@ehu.es
†francesca.baletto@kcl.ac.uk

the local structure and shape of Pt-clusters encapsulated in zeolite materials,[19,20] but the same authors have suggested that a local analysis, as opposed to an average characterisation, is needed to elucidate the structure-performance relationship. On this regard, atomistic simulations offer an extremely powerful tool. For the first time, we are going to argue that the observed magnetic dispersion originates from an ensemble of isomers taken from a proper selection of free NPs. We first identify 13 isomers fulfilling the geometrical constraints of the experiment. In the gas phase, most of these clusters are magnetically active. Assuming that each isomer, which can be accommodated in the zeolite, is equally likely grown, we show that only 30% of the isomers remain magnetically active, i.e., they present a total magnetisation equal or larger than 6 μ_B.

Theoretical studies of metallic NPs in porous frameworks such as zeolites are usually both scarce and limited to one or a few atoms and to few geometrical shapes.[21–24] Recent density-functional theory (DFT) calculations have suggested a Pt-icosahedron (Ih) as the shape grown inside zeolite pores.[25] Nevertheless, in gas phase, this geometry is energetically unfavourable with respect to the buckled pyramid (BP),[26] the triangular prism (TP),[27] and the low-symmetry shape (LOW) proposed by Piotrowski et al.,[28] which is currently identified with the local minimum. A complete structural description of Pt_{13}-NPs inserted into nanoporous materials is missing but highly desirable because it provides insights into how the embedding affects the structural stability of each isomer and, in turn, how this influences the magnetic nature of the sample.

Here, the physical properties of a variety of encaged Pt_{13} structures are calculated by DFT simulations which include van der Waals dispersion forces (DFT-D). As paradigmatic example of porous material, a 1:4 Al/Si faujasite super-cage, $H_{30}O_{42}Al_6Si_{24}$, containing two Al atoms per oxygen six-ring sub-structure is used as a matrix. For the first time, we demonstrate that Pt-NPs@NaY are anchored to the super-cage through just one atom and that their structural stability depends strongly on the solid angle at that anchor. When the solid angle is greater than 2 sr, i.e., for the Ih, the isomer undergoes a severe structural reconstruction. When we include van der Waals corrections, a new concave structure delimited by several square facets emerges as the optimal geometry, although it is unstable in the gas phase. Among the collection of more than 15 isomers that can be inserted into a zeolite pore, the number of highly coordinated and highly magnetic ($S > 3$) clusters decreases from the 70% in the gas phase to 30% after the embedding, due to structural changes leading to low coordinated shapes. A common strategy to investigate the magnetism of NPs is the concept of "superatom",[29–31] Namely the ability of a NP to behave like a large atom, showing degenerate energy levels labelled with proper quantum numbers. It is clear that such an approach works best for almost spherical clusters, where the degeneracy associated with the high symmetry of the underlying charge distribution and potential, allows for these quantum numbers to be conserved. In general, however, we have observed that among the 50 minima accessible to Pt_{13}, only the Ih could be described by this model. Almost all the others show low symmetry, therefore their energy levels are non-degenerate, and a superatom picture cannot be applied.[32] We refer the reader to the Supporting Information for further details and a figure of the energy levels of some of the clusters under investigation. Moreover, our preliminary calculations show that the total magnetisation is considerably reduced when Pt NPs are hydrogenated even in the gas phase. We expect that hydrogenation can affect in a similar way the encaged Pt NPs. (These results will be presented elsewhere.)

Model and Results

Considering that to numerically investigate the dynamical formation of the Pt_{13} in zeolites is still not yet feasible, we start with investigating all the possible stable isomers in the gas phase. Of these, only a few can be accommodated in the zeolite, due to geometrical constraints and the observed coordination number. We then introduce these clusters in the zeolite pore, and study both their magnetic and structural behaviour. In this analysis, we include all the clusters compatible with the constraints, augmented with the lowest energy isomer in the gas phase, LOW, and the Ih motif, immaterial of their energetic stability, since we do not know, a priori, either any kinetic trapping and/or the activation barrier between any pair of structures. Indeed, some of the energetically unfavourable isomers might exist when forming in the zeolite as metastable configuration with a lifetime long enough to be observed and measured. Therefore, we consider each of the isomers in our analysis equally likely to be formed in the zeolite pore.

Our numerical approach entails four different steps: accurate sampling of the potential energy surface of Pt-NPs in the gas phase with a focus on shapes with a high CN (larger than 5.3) throughout an

iterative metadynamics (iMT) calculation; refinement of the structural and magnetic properties within a DFT framework; selection and embedding of selected clusters within a NaY-zeolite pore; finally, characterisation of the structural and magnetic properties of the embedded clusters including van der Waals forces.

Metadynamics is a numerical algorithm used to accelerate rare events, where the ionic dynamics is biased by a history-dependent potential built on a set of reaction coordinates called collective variables.[33] Commonly used to explore free-energy surfaces, metadynamics has been recently proposed for sampling the energy landscape of small clusters.[34] To ensure a detailed sampling of shapes in the gas phase, an iMT employing the CN as unique collective variable, at temperatures as low as 5 K, is used as in Ref. 35. The first starting configurations are well-known geometries, such as LOW, BP, truncated bipyramid (TBP), TP, Ih, cubo-octahedron, and decahedron (Dh). When a morphology belonging to a new structural basin is obtained, this is quenched to its nearest local minimum and then used again as starting configuration for a new simulation, in an iterative manner. To speed up the structural search, a tight-binding second moment inter-atomic potential, able to reproduce the geometrical details of Pt clusters, is applied.[36] Anyway, at a second stage, the relative energy stability of each isomer is calculated according to the Broyden-Fletcher-Goldfarb-Shanno (BFGS) algorithm after relaxing the atomic structure to reduce the forces between each atomic pair, i.e., ionic relaxation, within a scalar-relativistic spin-polarized DFT framework, as available in the Quantum Espresso package.[37] Scalar-relativistic spin-polarized calculations with a non-linear core corrections and a small as 0.03 eV Marzari-Vanderbilt smearing are able to reproduce correctly the geometrical features and the magnetic moment of Pt_{13} especially when compared with relativistic approaches including spin-orbit coupling.[28,38] In the case of free NPs, the simulation box contains at least 13 Å of vacuum to avoid any spurious interaction between periodic images. While for encaged NPs in the zeolite cage, a cubic cell of approximately 28 Å is considered and a full BFGS ionic relaxation is used only for Pt atoms and the three inward O atoms of the six-ring substructure. Both standard DFT and corrected DFT for van der Waals forces, where a semi-empirical damp-dispersion term is introduced,[39] are performed. The NaY supercage does not exhibit any magnetic behaviour.

To mimic a faujasite supercage, a 1:4 Al/Si reduced model ($H_{30}O_{42}Al_6Si_{24}$) with at least two aluminium atoms per six-ring subunit has been considered. The whole crystalline structure is extracted from the accredited database of zeolite structures.[1] The fully periodic zeolite would contain more than 600 atoms, we are therefore in the position of considering only a part of it, namely only one pore. We assume therefore that the zeolite atoms outside this pore have negligible effect on the clusters. The suggested model has an available volume of 839 $Å^3$, where the latter is defined as the volume accessible to a spherical molecule after the van der Waals atomic sphere volumes are subtracted from the unit cell. When the Pt-O bond length is taken into account, this available volume indicates that an object with a maximum diameter of 7 to 8 Å, can be inserted into the pore. With respect to the Si/Al ordering in the zeolite, two models have been taken into account: one allows Al-O-Al bridges and the other respects the Löwenstein's rule, where only Si-O-Al fragments occur. In previous DFT studies, a periodically repeated Löwenstein's model was observed to be only slightly energetically more favourable than the Al-O-Al sequence.[40] Accordingly, our calculations revealed that the Al-O-Al fragment was comparable in energy to a Al-O-Si ordering (the latter is lower in energy by up to 0.2 eV). Moreover, some exemplary Pt_{13} clusters were inserted into the two Si/Al models. Their relative energy stability and their total magnetisation were not affected by the different order of Al atoms in the ring. We expect this result to hold true for all clusters that bind to the anchor in both models. However, we have noticed that the insertion of the cluster in the non Löwenstein's model cage produces structures with the lowest energies. Additionally, the anchoring point remains to one oxygen of the six-ring subunit. Therefore, in the following we report only the results obtained with the non-Löwenstein cage. More details and some analysis of the Löwenstein cage can be found in the Supporting Information. As a side note, we are currently exploring the validity of the Löwenstein's rule in a complete periodic NaY structure with and without the inclusion of Pt_{13} clusters. Indeed, it has been recently reported that the Löwenstein's rule might be broken for certain zeolites.[41] That analysis lies outside the realm of this work.

We first discuss the results for the gas phase. Figure 1 summarises the exhaustive sample of all the different local minima, labelled as "F" followed by a number, as obtained by the empirical-potential-driven iMT search followed by the DFT ionic relaxation, plotting their average CN -defined

[1] http://www.iza-structure.org/databases/

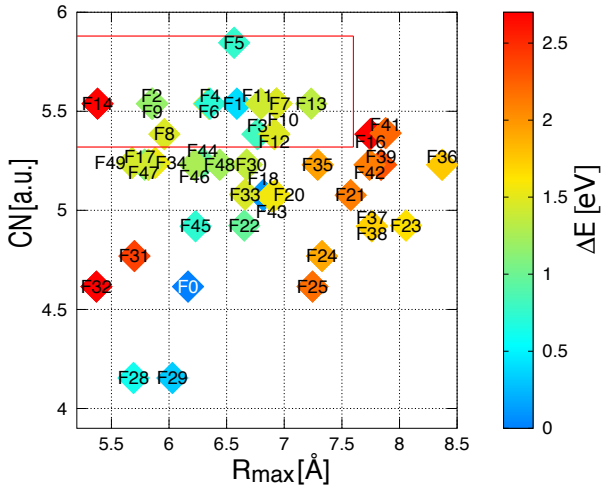

Figure 1: Energy stability of Pt_{13} isomers with respect to the global minimum (F0) plotted as a function of their coordination number, CN and maximum pair distance R_{max} in Å. The red box features isomers satisfying geometrical requirements.

as $\sum_{i|CN(i)<12|} CN(i)/13$, where $CN(i)$ is the coordination number of atom i (see also the Supporting Information)- against their maximum atomic pair distance (R_{max}, in Å). The colour scheme refers to their relative energy stability, ΔE, with respect to the LOW shape (F0), which is confirmed to be the energy global minimum in agreement with Piotrowski et al.[28]

The geometrical features of Pt-NPs embedded in NaY-zeolite, as reported in Refs.,[15,17,20] can be summarised as follows: (i) The average coordination number (CN) reaches a peak of 5.6, according to an analysis based on Fourier transform of the EXAFS χ(k) signal; (ii) the chemisorption site is on top of the oxygen six-ring site (SII); and (iii) the diameter should fit the dimensions of the cavity, and therefore be between 6 and 8 Å, and have a rather spherical shape. Indeed, noticing that the pore radius is about 13 Å, a maximum pair distance of about 7.5 Å represents the longest distance that can be accommodated in the supercage pore, since we need to take into account the Pt-O bond length and the O and Pt van der Waals radii. For the sake of completeness, F0 will be considered in our analysis despite having a very low CN. Notably, the other low-energy isomers, such as the two triangular prisms (F28 and F29), and the buckled pyramid (F18) exhibit CNs that are excessively low with respect to the experimental data and thus will be not considered further. The red box in Fig. 1 identifies the 14 isomers, F1 to F14, that satisfy those geometrical constraints.

For the sake of clarity, of the selected 15 clusters, we report in the first column of Fig. 2 only F0, F1 (also known as TBP, an incomplete Dh_{23}), F2 (belonging to the TP family and in the past proposed as the global minimum), and F14. Structure, energy stability, magnetisation, and average CN of all the others can be found in the Supporting Information grouped according to their geometrical taxonomy based on an atomic pair characterisation.[35] At the same time, we here briefly describe them. The family of the incomplete decahedron of 23 atoms, iDh_{23}, has four isomers without fivefold vertex -the TBP (F1), F3, and the stellated half-star shape, F4- and only one preserving a fivefold vertex (F13). A three-fold symmetric tri-augmented triangular prism (TTP), tagged F2, and the Dada-TTP (F6), belong to the same family. Three isomers -F5, F7, and F12- are incomplete double icosahedra of 19 atoms, $idIh_{19}$. Three helicoidal shapes -F8, F10, and F11-, a bi-layer geometry (F9) -the only fully crystallographic local minimum-, and the Ih_{13} (F14) complete the considered ensemble of Pt_{13}. Notably, only F1 has a ΔE below 0.5 eV while all the other isomers, but Ih, lying between 0.6 and 1.5 eV. With respect to magnetic properties, all the selected free Pt_{13} clusters show a ferromagnetic character. Their total magnetisation (TM), calculated as the difference between the majority and minority charge densities integrated over real space, is reported in Figs. 2 and 3. (See also the Supporting Information for all the other clusters.) The F0-F14 sample has an average TM of 5.6 μ_B, with roughly 45% of the isomers with a TM of 6 μ_B.

Notably, wire-like shapes such as F41 and F42, which arise from the interpenetration of octahedra of 6 atoms, have a very high TM (10-12 μ_B). Unfortunately, these shapes are too elongated ($R_{max} \sim 8$ Å) to be encapsulated into the supercage. At the same time, if we attempt to describe the set of all the isomers under investigation as super-atom, the Woods-Saxon potential and its energy level distribution as well as other models, considering there are 130 electrons in the valence band, predict, taking into account also the possibility of a Jahn-Teller distortion to lift level degeneracy, a total magnetisation ranging between 2 to 8 μ_B as we have observed for most of our clusters. [42]

Each of the F0-F14 isomers is then inserted into the NaY zeolite at the SII supercage site, and ionically relaxed, i.e., we let the atomic position change in order to minimise the total residual forces. As depicted in Fig. 2 and in the Supporting Information, with a "Z" we identify the embedded isomers in zeolite using a standard DFT framework, whereas "D" stand for the case where London dispersion corrections are included. A label R indicates isomers that reconstruct significantly from their starting configuration. We first note that, each isomer we have considered always chemisorbs through one Pt vertex anchored to only one O atom of the six-ring of the supercage, in very good agreement with experimental data. The relative stability of each minimum is calculated with respect to the lowest energy configuration, Z0-c and D0R-c, at DFT and DFT-D, respectively. In Fig. 3, free and encaged minima are plotted as functions of their CN and TM, and the colour scheme refers to their energy stability with respect to the most favourable isomer at this level of the theory. At the DFT level, the overall coordination of Pt clusters, and thus their magnetic properties, is almost preserved after the isomers are embedded with the exception of those undergoing a major reconstruction, i.e., Z6R, Z7R, Z8R, Z13R, and Z14R.

Within a DFT-D framework, the net effect of adding dispersion forces is a decrease in the nearest-neighbor average distance, a preference for forming a cage-like shape associated with a higher binding energy, and the shift towards lower coordinated isomers as made evident in Fig. 3. Compared with the DFT case, the distance between the anchor and the center of the oxygen ring is always shorter by 0.1-0.3 Å. Simultaneously, all the embedded NPs tend to move toward the center of the cage, where the average distance between the cluster centers of mass and the geometrical center of the pore is 0.2-0.3 Å. The dispersion forces thus induce a few local atomic rearrangements that are sometimes significant. The most relevant case is the global minimum Z0-c. Indeed, D0R-c, which is an L-shaped motif delimited by six squares linked to the supercage through a three-fold vertex, arises from Z0-c when dispersion forces are introduced. Notably, D0R-c is unstable in the gas phase and folds again into the original LOW shape. However, its counterpart chemisorbed with a three-fold vertex, D0-b, remains geometrically stable, although it loses 0.4 eV in energy. At the DFT-D level, the ΔE is spread up to 2.5 eV and it is strongly correlated to the coordination number where $\Delta E > 1.5$ eV are for CN > 4.7.

Discussion and Conclusions

To fully understand the geometrical stability of zeolite-embedded Pt-NPs, we investigate the role of the vertex anchoring the cluster to the supercage. At the DFT level, the chemisorption through a 3- and 4-fold coordinated vertex usually leads to negligible changes in the overall cluster shape, whereas chemisorption through a 5-fold coordinated vertex leads to major structural transformations. To be more quantitative, the encapsulation energy E_{enc} and the solid angle at the anchor, Ω, were calculated. E_{enc} is the energy gain due to the embedding, where values greater than 1.3 eV indicate structural rearrangement of the whole cluster. The values of Ω reported per each isomer in Fig. 2 represents the angles subtended by the polygon obtained by connecting all the Pt atoms coordinated to the vertex, as projected onto the unit sphere around it. Our simulations show that only solid angles Ω smaller than 0.8 sr are fully stable, while values greater than 2 sr are completely unstable from a geometrical point of view; i.e., the polygon underneath the vertex/anchor can be a triangle or a quadrilateral, but not a rectangle or planar pentagon. Among clusters with $\Omega < 0.8$ sr, the best examples are the truncated bi-pyramid (Z1) and the symmetric TTP-based structure (Z2); they have a three-fold rotational symmetry around the Pt-anchor, and a $E_{enc} \sim 0.9$ eV. A non-planar pentagon, with a borderline value of Ω, is allowed, as in the case of the bilayer (Z9) which has a $E_{enc} \sim 0.9$ eV. When $\Omega > 2$ sr and $E_{enc} > 1.4$ eV, severe rearrangements occur to decrease Ω to approximately 1 sr, as depicted in Fig. 2. Generally speaking, structural reconstructions lower the TM with the sole exception of the isomer arising from the

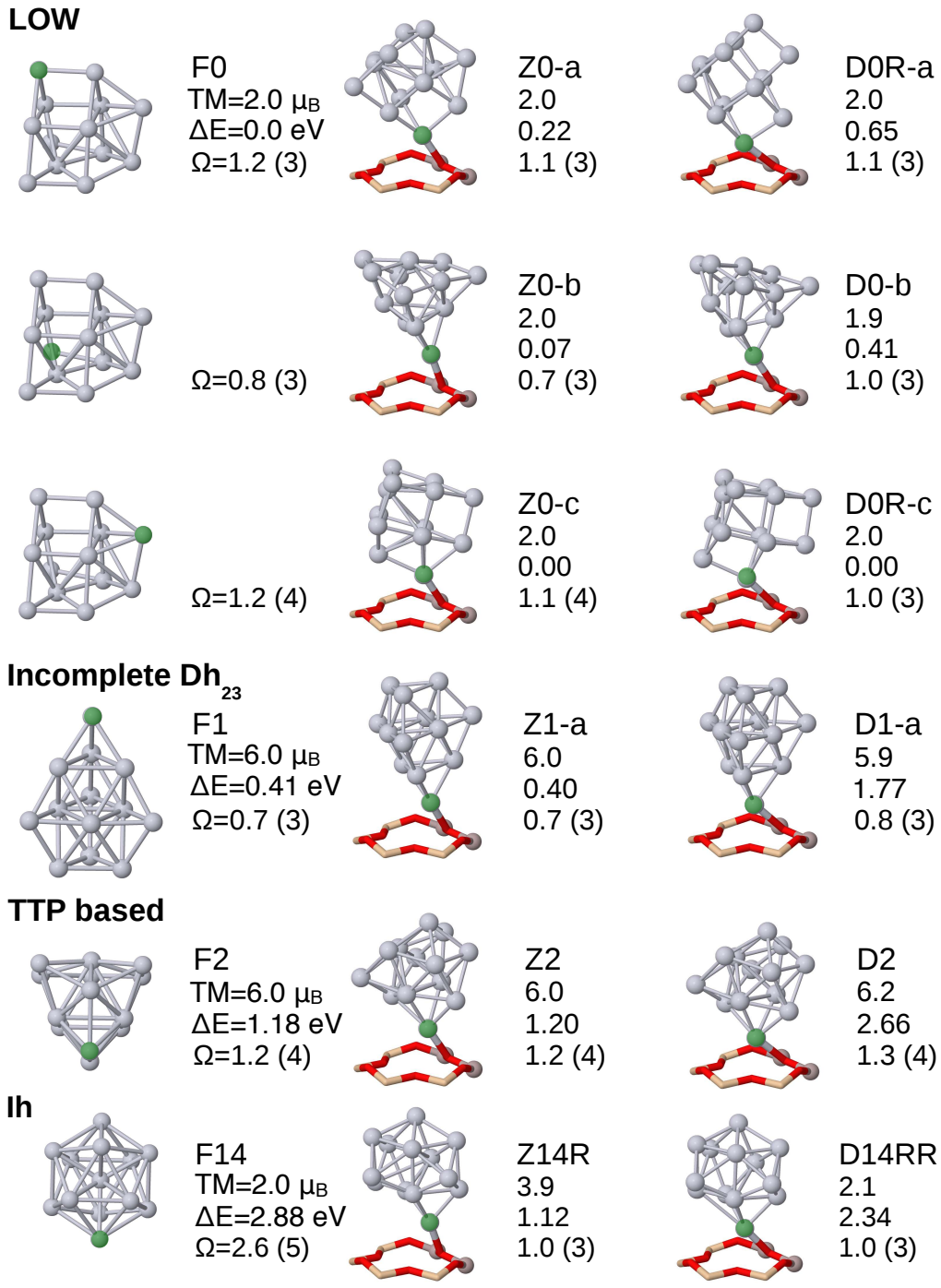

Figure 2: Selected Pt_{13} isomers, classified into their geometrical families. The left columns represents the gas phase (F prefixes), the middle column represents Pt_{13} inserted into the zeolite supercage (Z prefixes); and the third column represents refinement at the DFT-D level (D prefixes). For each cluster, the total magnetisation in Bohr magneton (μ_B), the relative energy with respect the global minimum (in eV), and the solid angle at the anchor are listed below their identification label. The coordination of the anchor itself is listed in brackets. Data visualised using VESTA.[43]

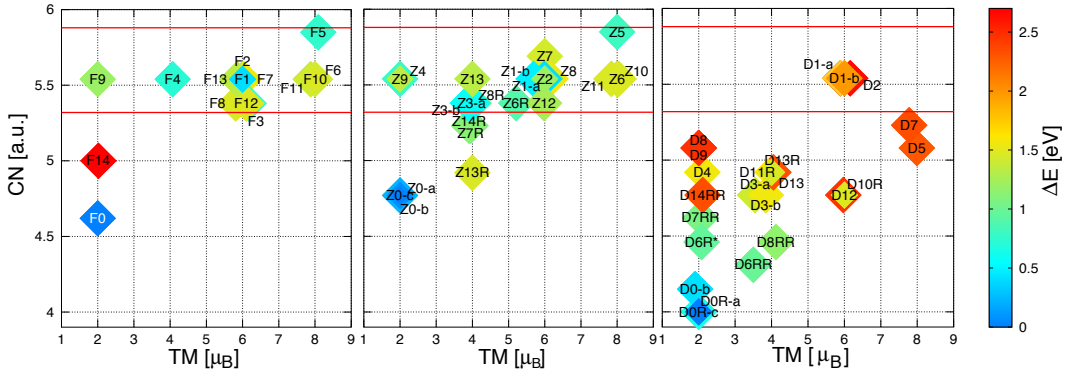

Figure 3: Average coordination number (CN) with respect to the total magnetisation, TM (μ_B). The colour refers to energy stability of Pt13 -NPs in the gas phase (left), embedded in an NaY zeolite (middle) and in zeolite with dispersion forces DFT-D (right). ΔE (eV), relative energy stability, to the global minima F0, Z0-c and D0R-c, respectively. The region between the red lines identifies the experimental range of coordination.

Ih. Notably, the Ih_{13} indeed evolves towards a iDh_{23} upon a three-fold anchor, a distorted half-star, Z4. Not surprisingly, the reconstructed Ih exhibits a TM of 4 μ_B similarly to Z4. Those structures that reconstructed at the DFT level because of the embedding continue to change toward less coordinated shapes at the DFT-D level. Notably, the incomplete decahedra are geometrically stable while helicoidal shapes tend to rearrange. However, we want to point out that we are not investigating the free energy landscape of encapsulated Pt_{13}, i.e., besides a simple energetic argument following an ionic relaxation, we cannot establish how easy is to transform from one shape into another and we have no access to the activation energy barrier required for these structural changes. Anyway, a few details of those solid-solid reconstructions are provided in the Supporting Information. In the following, we are going to assume that each of these structures is equally likely embedded in the zeolite pore. We have also calculated the spin density difference to show that for high-magnetic clusters (D1-a and D2), the majority spin density accommodates mostly on the shell, while for low-magnetic clusters (D0R-c and D14-RR) the spin density does not show a precise character and we have the accumulation of both spins on the shell, see Fig. 4. We also notice that there is a significant spin accumulation at the anchor between the NP and the cage. This plausibly suggests some charge transfer with the anchor during the formation process. However, it seems that the nature of this latter spin accumulation does not influence the overall magnetic character, since D2 and D1-a show similar magnetism. There is some small minority spin accumulation in the zeolite for the D0R-c away from the anchor (see Fig. 4 upper left corner). We notice however that this is probably a second order small effect, since there is not a chemical bond between the Pt atom and the zeolite cage at that point, since the atomic distance is larger than 3.5 Å.

The estimated of the gap between the highest occupied and the lowest unoccupied molecular orbital of a few selected clusters in zeolite varies between 4.5 to 5 eV for all the clusters we have analysed. The highest occupied Kohn-Sham state is shown in Fig. S4 for some selected clusters: we notice that this state localises almost completely on the NP, with some hybridisation with the states of the O at the anchor. Anyway a deeper understanding of structural changes of Pt-NPs embedded in zeolite is needed although out of the purpose of this article.

The structural rearrangements due to the embedding and the inclusion of van der Waals forces strongly affect the magnetic properties of Pt_{13}-NPs@NaY. Although TM ranges between 2 and 8 μ_B as in the gas phase, the average TM is about 3.9 μ_B against 4.8 μ_B at the DFT level, and 5.6 μ_B in the gas phase, as shown in Fig. 5. From this figure, we can see that the observed small fraction of magnetically active isomers in the NaY can be justified by observing that embedding in the zeolite cage strongly modifies the magnetic distribution. Our calculations show that this result does not depend on the oxygen bridge (Al-O-Al or Si-O-Al) we have assumed in the six-ring subunit where the cluster anchors. Assuming that each of the clusters we have investigated in the zeolite is equally likely synthesised, we observe that overall only about 30% of the isomers are magnetically active with a TM>6 μ_B. The decrease in the TM is associated to the stabilisation of low coordinated shapes. D7 is the only case which increases its

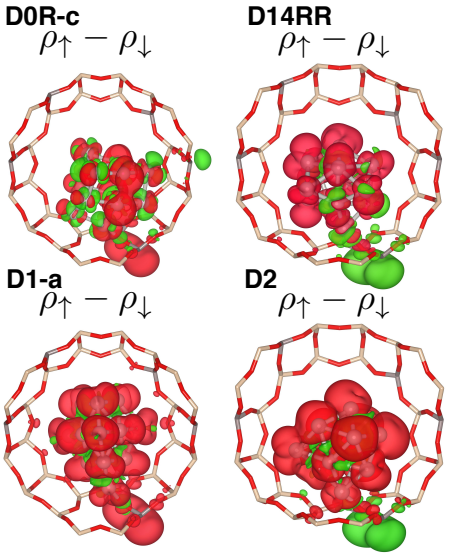

Figure 4: Spin density ($\rho_\uparrow - \rho_\downarrow$) for 4 Pt_{13} isomers (D0R-c which is the ground state, D2, D1-a, and D14-RR), drawn with a iso-surface level of ± 0.0005 Å^{-3}. In red the positive value, in green the negative values. Data visualised using VESTA.[43]

TM to 8 μ_B due to a different orientation within the supercage. Thus far, at the DFT-D level, only six isomers have a TM above 6 μ_B: TBP (D1); TTP (D2); iIh_{19} (D12) and the helicoidal D10-R, which have a spin state of 3; and the other two incomplete icosahedra D5 and D7 which show a high magnetisation of 8 μ_B. Anyway, only four of them are highly coordinated (CN>5).

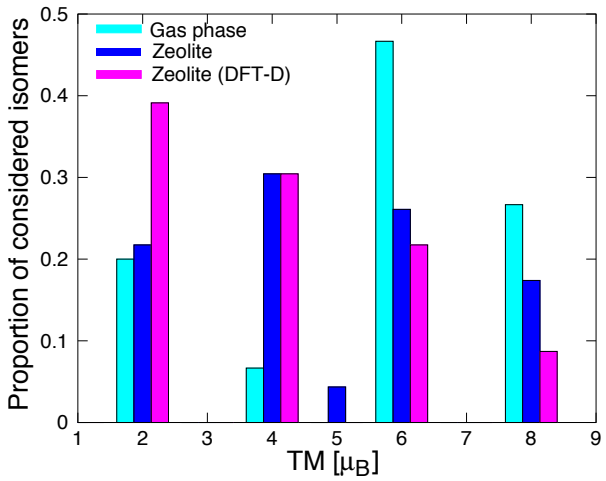

Figure 5: Proportion of considered isomers in terms of their total magnetisation TM (μ_B), in the gas phase (cyan), in zeolite (blue) and DFT-D zeolite (magenta).

Bartolomè and co-workers[17] suggested that the magnetic behaviour of Pt-NPs could be influenced by a charge-transfer between the O atoms of the cage and the cluster. Here, we observe a charge transfer of approximately 0.2 e^-/atom from the O toward the Pt vertex bound to the six-ring substructure. The involved oxygen exhibits an atomic polarisability of $\pm$ 0.4 μ_B that contributes to the total magnetic moment of the whole system. The presence of two Al atoms close to the vertex/anchor of the NP results in a Pt-O distance peaked at 2.25 Å in excellent agreement with experiments.[15] (See also Fig. S3 where we report the Bader charge analysis for the Pt13 clusters loaded in zeolite.)

In conclusion, we investigated the energy landscape of Pt_{13} using a metadynamics approach and found an exhaustive set of highly coordinated isomers with a maximum pair distance shorter than 7.5

Å. Fifteen different isomers were selected and then embedded in a NaY zeolite supercage model with different orientations when possible. Each Pt_{13}-NP adsorbs at the SII site with a vertex anchored to the inward O atom of the six oxygen ring substructure. The effect of the embedding was the destabilisation of NPs linked to the supercage throughout solid angles larger than 2 sr, as occurs in the case of the icosahedron. Long-range van der Waals forces were included to determine the stability of each isomer, and their magnetic properties were subsequently estimated. In the case of encapsulated Pt-NPs, a new concave structure was found to be the lowest energy structure. As in the gas phase, the embedded Pt-NPs exhibit a magnetic behaviour, with a total magnetisation between 2 and 8 μ_B, somewhat in agreement with a super-atom model. However, due to the stabilisation of low coordinated isomers, the majority exhibits a TM of 2 μ_B against a value of 6 μ_B calculated in free clusters (see Fig. 5). Moreover, we have considered also H chemisorption on the Pt cluster to compare better with experiments: we have found that the presence of H atoms reduces the TM for the clusters F0, F1, F2, and F14, and we expect a similar result to apply to all other isomers, both in the gas phase and in the zeolite. (These results will be presented elsewhere.) A charge transfer between the zeolite cage and Pt atoms occurred when two Al atoms occupied vicinal positions in the six-ring substructure of the zeolite, leaving the oxygen atom between them slightly polarised. The high magnetic moment of Pt_{13} nanoparticles in zeolite, was mainly due to four highly coordinated shapes: a truncated bi-pyramid, a triaugmented triangular prism, and two incomplete double icosahedra, which represent the 30% of a sample where all the isomers have the same probability to be inserted in the pore. This explains why only a fraction of the total Pt load is magnetically active in very good agreement with available experimental data.

Acknowledgement. This work was supported by the U.K. research council EPSRC, under Grant No. EP/GO03146/1. R.D'A. acknowledges financial support by DYN-XC-TRANS (Grant No. FIS2013-43130-P) and SElecT-DFT (Grant No. FIS2016-79464-P), the Grupo Consolidado UPV/EHU del Gobierno Vasco (IT578-13), and NANOTherm (CSD2010-00044) of the Spanish Ministerio de Economia y Competitividad. The authors would like to thank A. Floris and A. Comisso for their useful suggestions. C.D.P., L.P., and F.B. acknowledge support from the COST Action MP0903 "Nanoalloys as Advanced Materials: From Structure to Properties and Applications". We also acknowledge computational time from the Barcelona SuperComputing Centre through the project QCM-2017-2-0010 and from the Donosti International Physics Centre.

Supporting Information Available. A full description of the adopted computational procedure, a table as in Fig. 2 for all the selected 14 isomers is present (see Fig. S1),we report the energy stability and a Bader charge analysis (see Fig. S2), the analysis of the pair distance distribution function in the zeolite (Fig. S3), a plot of the spin densities and the highest occupied molecular orbital (fig. S4). Finally Fig. S5 reports the energy levels of some isolated clusters. Moreover, structural features of zeolite cages and details of structural instability of embedded Pt-NPs could be found in the Supporting Information.

References

[1] A. Chen and P. Holt-Hindle, *Chem. Rev.*, 2010, **110**, 3767.

[2] A. Barnard, *Rep. Prog. Phys.*, 2010, **73**, 086502.

[3] C. M. Sánchez-Sánchez, J. Solla-Gullón, F. J. Vidal-Iglesias, A. Aldaz, V. Montiel and E. Herrero, *J. Am. Chem. Soc.*, 2010, **132**, 5622–5624.

[4] V. M. Medel, J. U. Reveles, S. N. Khanna, V. Chauhan, P. Sen and A. W. Castleman, *Proc. Natl. Acad. Sci.*, 2011, **108**, 10062–10066.

[5] C. Di Paola, R. D'Agosta and F. Baletto, *Nano Lett.*, 2016, **16**, 2885–2889.

[6] Y. Guo, J. Hu and L. Wan, *Adv. Materials*, 2008, **20**, 2878.

[7] J. Chen, B. Lim, E. P. Lee and Y. Xia, *Nano Today*, 2009, **4**, 81–95.

[8] J. Zečević, A. M. J. van der Eerden, H. Friedrich, P. E. de Jongh and K. P. de Jong, *ACS Nano*, 2013, **7**, 3698–3705.

[9] C. Koenigsmann, A. C. Santulli, K. Gong, M. B. Vukmirovic, W.-P. Zhou, E. Sutter, S. S. Wong and R. R. Adzic, *J. Am. Chem. Soc.*, 2011, **133**, 9783–9795.

[10] Y. Sakamoto, Y. Oba, H. Maki, M. Suda, Y. Einaga, T. Sato, M. Mizumaki, N. Kawamura and M. Suzuki, *Phys. Rev. B*, 2011, **83**, 104420.

[11] I. Parsina, C. Di Paola and F. Baletto, *Nanoscale*, 2012, **4**, 1160.

[12] C. Di Paola and F. Baletto, *Eur. Phys. J. D*, 2013, **67**, 49.

[13] A. Smogunov, A. Dal Corso, A. Delin, R. Weht and E. Tosatti, *Nat. Nanotechnol.*, 2008, **3**, 22.

[14] U. Maitra, B. Das, N. Kumar, A. Sundaresan and C. Rao, *Chem. Phys. Chem.*, 2011, **12**, 2322.

[15] X. Liu, M. Bauer, H. Bertagnolli, E. Roduner, J. van Slageren and F. Phillipp, *Phys. Rev. Lett.*, 2006, **97**, 253401.

[16] X. Liu, M. Bauer, H. Bertagnolli, E. Roduner, J. van Slageren and F. Phillipp, *Phys. Rev. Lett.*, 2009, **102**, 049902 (E).

[17] J. Bartolomé, F. Bartolomé, L. M. Garcia, E. Roduner, Y. Akdogan, F. Wilhelm and A. Rogalev, *Phys. Rev. B*, 2009, **80**, 014404.

[18] X. Batlle, N. Perez, P. Guardia, O. Iglesias, A. Labarta, F. Bartolomé, L. M. Garcia, J. Bartolomé, A. G. Roca, M. P. Morales and C. J. Serna, *J. App. Phys.*, 2011, **109**, 07B524.

[19] E. Roduner, C. Jensen, J. van Slageren, R. A. Rakoczy, O. Larlus and M. Hunger, *Angew. Chemie - Int. Ed.*, 2014, **53**, 4318–4321.

[20] Y. Akdogan, C. Vogt, M. Bauer, H. Bertagnolli, L. Giurgiu and E. Roduner, *Phys. Chem. Chem. Phys.*, 2008, **10**, 2952.

[21] O. Bunau, J. Bartolomé, F. Bartolomé and L.-M. Garcia, *J. Phys. Condens. Matter*, 2014, **26**, 196006.

[22] S. Yadnum, S. Choomwattana, P. Khongpracha, J. Sirijaraensre and J. Limtrakul, *ChemPhysChem*, 2013, **14**, 923–928.

[23] J. A. Huertas-Miranda and M. M. Martinez-Inesta, *Molecular Simulation*, 2013, **39**, 176.

[24] B. Boekfa, S. Choomwattana, P. Khongpracha and J. Limtrakul, *Langmuir*, 2009, **25**, 12990–12999.

[25] X. Liu, H. Dilger, R. Eichel, J. Kunstmann and E. Roduner, *J. Phys. Chem. B*, 2006, **110**, 2013.

[26] C. H. Hu, C. Chizallet, H. Thoulhoat and P. Raybaud, *Phys. Rev. B*, 2009, **79**, 195416.

[27] L.-L. Wang and D.-D. Johnson, *Phys. Rev. B*, 2007, **75**, 235405.

[28] M. J. Piotrowski, P. Piquini and J. L. F. Da Silva, *Phys. Rev. B*, 2010, **81**, 155446.

[29] A. Castleman and S. Khanna, *J. Phys. Chem C*, 2009, **113**, 2664–2675.

[30] J. U. Reveles, P. A. Clayborne, A. C. Reber, S. N. Khanna, K. Pradhan, P. Sen and M. R. Pederson, *Nat. Chem.*, 2009, **1**, 310–315.

[31] E. Roduner and C. Jensen, *Magnetochemistry*, 2015, **1**, 28–44.

[32] A. C. Reber and S. N. Khanna, *Accounts of Chemical Research*, 2017, **50**, 255–263.

[33] A. Laio and M. Parrinello, *Proc. Natl. Acad. Sci. U.S.A.*, 2002, **99**, 12562.

[34] G. A. Tribello, J. Cuny, H. Eshet and M. Parrinello, *J. Chem, Phys.*, 2011, **135**, 114109.

[35] L. Pavan, C. Di Paola and F. Baletto, *Eur. Phys. J. D*, 2013, **67**, 24.

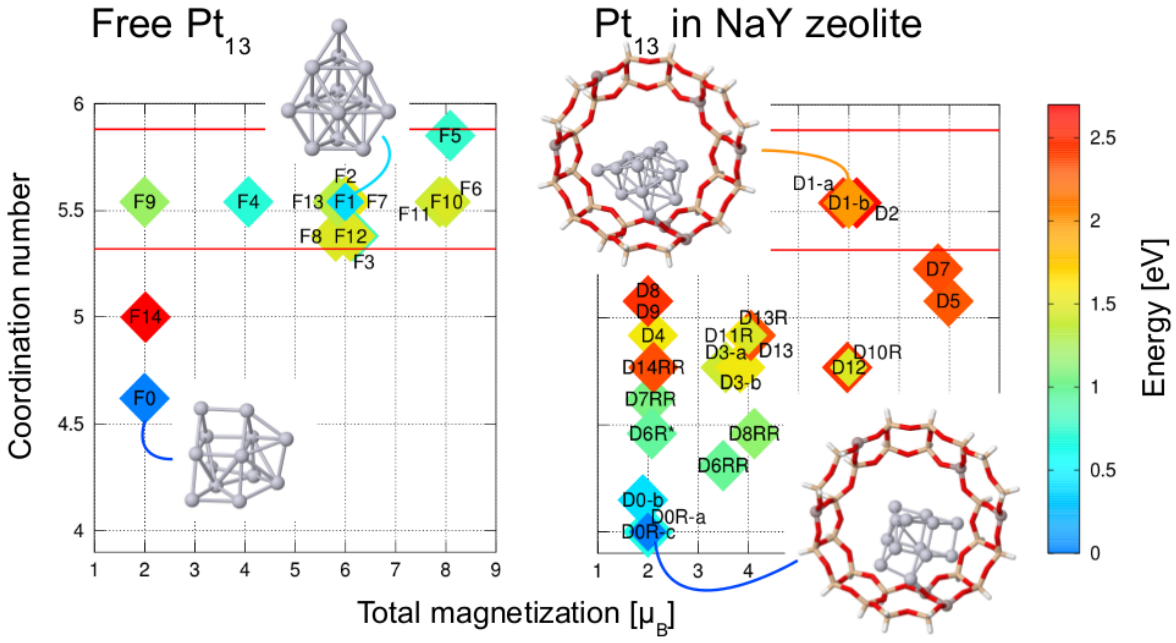

[36] F. Baletto, R. Ferrando, A. Fortunelli, F. Montalenti and C. Mottet, *J. Chem. Phys.*, 2002, **116**, 3856.

[37] P. Giannozzi, S. Baroni, N. Bonini, M. Calandra, R. Car, C. Cavazzoni, D. Ceresoli, G. L. Chiarotti, M. Cococcioni, I. Dabo, A. Dal Corso, S. de Gironcoli, S. Fabris, G. Fratesi, R. Gebauer, U. Gerstmann, C. Gougoussis, A. Kokalj, M. Lazzeri, L. Martin-Samos, N. Marzari, F. Mauri, R. Mazzarello, S. Paolini, A. Pasquarello, L. Paulatto, C. Sbraccia, S. Scandolo, G. Sclauzero, A. P. Seitsonen, A. Smogunov, P. Umari and R. M. Wentzcovitch, *J. Phys. Condens. Matter*, 2009, **21**, 395502.

[38] P. Blonski and J. Hafner, *J. Phys.-Condens. Matter*, 2011, **23**, 136001.

[39] V. Barone, M. Casarin, D. Forrer, M. Pavone, M. Sambi and A. Vittadini, *J. Comput. Chem.*, 2009, **30**, 934–939.

[40] R. Bell, R. Jackson and C. Catlow, *Zeolites*, 1992, **12**, 870.

[41] R. E. Fletcher, S. Ling and B. Slater, 2016, arXiv:1612.04162.

[42] D. Bonatsos, N. Karoussos, D. Lenis, P. P. Raychev, R. P. Roussev and P. A. Terziev, *Phys. Rev. A*, 2000, **62**, 013203.

[43] K. Momma and F. Izumi, *J. Appl. Crystallogr.*, 2011, **44**, 1272–1276.